Au@Ag@Pt core-shell nanorods regulating Ag release behavior endow titanium antibacterial activity and biocompatibility

Jiajun Qiu[1, 3, #], Tingting Yang[2, 3, #], Yifan Li[4], Wenhao Qian[5, *], Xuanyong Liu[1, 3, *]

[1] School of Chemistry and Materials Science, Hangzhou Institute for Advanced Study, University of Chinese Academy of Sciences, 1 Sub-lane Xiangshan, Hangzhou, 310024, China

[2] College of Materials Science & Engineering, Jiamusi University, Jiamusi 154007, China

[3] State Key Laboratory of High Performance Ceramics and Superfine Microstructure, Shanghai Institute of Ceramics, Chinese Academy of Sciences, Shanghai, 200050, China

[4] Smart Materials and Surfaces Laboratory, Faculty of Engineering and Environment, Northumbria University, Newcastle upon Tyne, NE1 8ST UK

[5] Shanghai Xuhui District Dental Center, Shanghai 200032, China

[#] These authors contributed equally to this work.

[*]Correspondence: xyliu@mail.sic.ac.cn (X. Liu), pingyanlaoto@163.com (W. Qian)

Abstract: Although titanium and its alloys are extensively used in orthopedics and dentistry fields, implant failures still happen because of implant-associated infections. Herein, Au@Ag@Pt core-shell nanorods with noble metal combination were fabricated and assembled on medical titanium surface and the antibacterial activity and biocompatibility were investigated. The results showed that antibacterial rates of Ti-Au@Ag@Pt against *S. epidermidis* and *P. aeruginosa* were 89.7% and 92.7%, respectively. Besides, Ti-Au@Ag@Pt showed no obvious cell toxicity with MC3T3-E1 cells grew well on the sample surface. It was discovered that the Pt shell layer on Ti-Au@Ag@Pt slowed down the Ag ion release rate which endowed medical titanium surface with both antibacterial activity and good biocompatibility.

Keywords: titanium, silver, nanorod, antibacterial, biocompatibility

1. Introduction

Titanium and its alloys are extensively used in orthopedics and dentistry fields due to their superior physicochemical properties and good biocompatibility [1]. Despite the advantages, implant-associated infection, one of the most severe post-surgery complications, still occurs which will lead to implant failure [2]. To address this problem, it is necessary to endow titanium implants with antibacterial activity. Thus, surface modifications are needed to improve the success rate of titanium implants by introducing antibacterial agents including antibiotics, inorganic, or organic bactericidal coating [3-8].

However, antibiotic resistance has become a public health threat due to the abuse of antibiotics [9]. Compared to antibiotics, silver (Ag) is an inorganic antibacterial agent which has a broad spectrum of antibacterial effect [7]. Due to their superior inhibitory and biocidal effects, Ag-based antibacterial agents attract wide attention [10-13]. Therefore, Ag-based antibacterial agents, in the form of metallic Ag or Ag ions, have been widely used as bactericides to treat various bacterial infections containing Gram-positive and Gram-negative bacteria. For example, Fan et al. developed an Ag-loaded mesoporous bioactive glass (Ag-MBG) and realized antibacterial effects against *Enterococcus faecalis* in root canal by releasing Ag ions from Ag-MBG [14]. Wei et al. prepared TiO_2 nanotubes with long-term antibacterial activity by loading Ag nanoparticles and Ag ions [15].

Although the antibacterial effects of Ag-based antibacterial agents are proved, challenges remain in their applications in medical implants. It is important to note

that the biocompatibility should not be ignored, as cytotoxicity was found resulting from Ag nanoparticles or Ag ions [16, 17]. Besides, Ag nanoparticles are easy to aggregate which in turn reduces their antibacterial efficiency. To address these issues, in the present work, Au@Ag@Pt core-shell nanorods with the noble metal combination were fabricated on the titanium surface. Au nanorods were acted as the carriers, metallic Ag were uniformly dispersed on the surface of Au nanorods, and Pt shell regulated the release behaviors of Ag ions which endow titanium with both antibacterial activity and good biocompatibility.

2. Materials and methods

2.1. Sample preparation

Gold nanorods (GNRs) were fabricated based on a seed-mediated growth method according to our previous work [18]. In brief, seed solutions were obtained after mixing 0.12 mL of $HAuCl_4$ solution (0.02 M, Aladdin, China), 5 mL of cetytrimethylammoium bromide solution (CTAB, 0.1 M, Aladdin, China), and 0.6 mL of $NaBH_4$ (0.01 M, Aladdin, China) under magnetic stirring. Subsequently, 1.5 mL of $HAuCl_4$ solution (0.02 M) and 0.8 mL of silver nitrate solution were introduced into 30 mL of CTAB solution (0.1 M). Then, 0.1 M of ascorbic acid (AA) solution (Aladdin, China) was introduced until the abovementioned solution turned colorless under magnetic stirring. At last, GNRs were obtained after adding 76 μL of as-prepared seed solution and reacted for 12 h.

To prepare Au@Ag core-shell structure nanorods, 55 μL of ascorbic acid solution (0.01 M), 0.2 mL of silver nitrate solution (0.01 M) and 50 μL of NaOH (0.1 M) were

introduced to the as-prepared GNRs solution (5 mL) with magnetic stirring for 1 h and the corresponding samples were denoted as Au@Ag. Au@Pt core-shell structure nanorods were fabricated by adding 0.9 mL of AA solution (0.01 M) and 20 μL of H_2PtCl_6 solution (18 mM, Sinopharm Group, China) into 6 mL of as-prepared GNRs solution and reacting for 1 h under magnetic stirring at 60 °C. The corresponding samples were indicated as Au@Pt. Similarly, to prepare Au@Ag@Pt core-shell structure nanorods, 0.9 mL of AA solution (0.01 M) and 20 μL of H_2PtCl_6 solution (18 mM) were added into 6 mL of as-prepared Au@Ag solution and reacted for 1 h under magnetic stirring at 60 °C. The corresponding samples were indicated as Au@Ag@Pt.

The self-assembly of GNRs, Au@Ag, Au@Pt, Au@Ag@Pt on medical titanium surfaces is as follows. First, pure titanium plates with the size of 10 × 10 × 1 mm^3 were cleaned with a mixed acid solution (volume ratio of HF: HNO_3: H_2O is 1: 5: 34). To obtain hydroxylated surfaces, these titanium plates were immersed in a piranha solution (volume ratio of H_2SO_4: H_2O_2 was 3: 1) for 3 h. Then, these titanium plates were transferred into 3-aminopropyltrimethoxysilane (APS) solutions (5 vol. %, Aladdin, China) and reacted under ultrasonic agitation for 2 h. The APS-treated plates were then transferred into NaCl solution (6 mM) containing polystyrensulfonate (PSS, 100mg/mL, Aladdin, China) for 24 h with shaking. At last, APS-PSS-treated plates were separately immersed into GNRs, Au@Ag, Au@Pt, and Au@Ag@Pt solutions and the corresponding samples were labeled as Ti-GNR, Ti-Au@Ag, Ti-Au@Pt, Ti-Au@Ag@Pt, respectively. The titanium plate treated with piranha solution was used as the control group and labeled as Ti.

2.2. Surface characterization

Surface morphologies of GNRs, Au@Ag, Au@Pt, Au@Ag@Pt were observed using transmission electron microscopy (TEM, HRTEM, JSM-6700 F, JEOL, Japan). The sizes of nanorods were calculated using ImageJ Software using TEM image scale bar as reference. Scanning electron microscopy (SEM, S-4800, Hitachi, Japan) was utilized to observe the surface topography of Ti, Ti-GNR, Ti-Au@Ag, Ti-Au@Pt, and Ti-Au@Ag@Pt. The surface elemental compositions and chemical states of Ti, Ti-GNR, Ti-Au@Ag, Ti-Au@Pt, and Ti-Au@Ag@Pt were detected by X-ray photoelectron spectroscopy (XPS, Physical Electronics PHI 5802). The absorption spectra of GNRs, Au@Ag, Au@Pt, Au@Ag@Pt were analyzed using a UV–Vis-NIR spectrophotometer (Lambda 750, PerkinElmer, USA). The surface contact angles of various samples were measured using a contact angle measurement (SL200B, China). To be specific, 2 μL of ultrapure water was dropped on each sample and the photo was taken with the built-in camera. Water contact angles were obtained after analyzing the photos.

2.3. Ag release assessment

Ti-GNR, Ti-Au@Ag, Ti-Au@Pt, and Ti-Au@Ag@Pt were separately immersed into 5 mL of ultrapure water at 37 °C for 7 days. The released Ag contents were measured by inductively coupled plasma atomic emission spectroscopy (ICP-AES).

2.4. Antibacterial activity analysis

Strains of *Pseudomonas aeruginosa* (*P. aeruginosa*, ATCC 27853) and *Staphylococcus epidermidis* (*S. epidermidis*, ATCC 12228) were utilized to assess the antibacterial activities of Ti, Ti-GNR, Ti-Au@Ag, Ti-Au@Pt, and Ti-Au@Ag@Pt. *P.*

aeruginosa and *S. epidermidis* were cultured with Luria-Bertani broth (LB) and tryptic soy broth (TSB), respectively. The various samples were sterilized under ultraviolet radiation for 12 h. Then, 60 μL of bacterial suspensions with a cell density of 1×10^7 CFU/mL were seeded on various samples and cultured for 24 h at 37 °C. For bacteria colony counting, bacteria on the sample surfaces were detached and collected in a 5 mL tube. Then, the detached bacterial suspension was serially diluted tenfold with physiological saline and 100 μL of diluted bacterial suspension was transferred to a standard agar culture plate for further cultivation for 24 h. Finally, photographs of agar culture plates were taken and the number of bacteria colonies were counted. The antibacterial rates were calculated according to the following formula:

$$\text{Antibacterial rate (\%)} = \frac{N_0 - N_1}{N_0} \times 100$$

Where N_0 presents the average number of bacteria colonies on the control sample (CFU/mL) and N_1 indicates the average number of bacteria colonies on the experimental sample. For SEM bacterial morphology observation, bacteria on the samples were fixed using 2.5% glutaraldehyde and dehydrated with gradient ethanol solutions and hexamethyl disilazane ethanol solution. At last, bacterial morphologies were observed using a scanning electron microscope (SEM, S-3400N, Hitachi, Japan). To figure out whether Ag ions release led to the antibacterial effect, an agar diffusion assay was carried out. In brief, 100 μL of bacterial suspension (1×10^7 CFU/mL) was introduced to the agar culture plates. Subsequently, Ti, Ti-GNR, Ti-Au@Ag, Ti-Au@Pt, and Ti-Au@Ag@Pt were placed on the agar culture plates and cultured at 37 °C for 24 h. At last, photographs of agar culture plates were taken.

2.5. Cytocompatibility evaluation

MC3T3-E1 cells (purchased from cells Resource Center, Shanghai Institutes of Biological Science, China) were utilized to investigate the cell viability of various samples. The MC3T3-E1 cells were cultured with Dulbecco's minimum essential medium (DMEM, Gibco, Invitrogen, Inc, USA) containing 10% fetal bovine serum (FBS, Gibco, Invitrogen, Inc, USA), 1% antimicrobial of penicillin-streptomycin (Antibiotic-Antimycotic, Gibco, Invitrogen, Inc, USA) with 5% CO_2 at 37 °C in a humidified atmosphere. The cell culture medium was refreshed every 3 days. All the samples were sterilized with ultraviolet radiation for 12 h. To evaluate the cell viability of Ti, Ti-GNR, Ti-Au@Ag, Ti-Au@Pt, and Ti-Au@Ag@Pt, 1 mL of MC3T3-E1 cells (5.0×10^4 cells/mL) were introduced on various samples and cultured for 1 day. Then, cells on samples were fixed using 2.5% glutaraldehyde and dehydrated with gradient ethanol solutions and hexamethyl disilazane ethanol solution. At last, cell morphologies were observed using a scanning electron microscope (SEM, S-3400N, Hitachi, Japan).

2.6. Statistical analysis

All the data were presented as the mean ± standard deviations. Statistical analysis was assessed using GraphPad Prism Software. The statistically significant differences were analyzed using a two-way analysis of variance and Tukey's multiple comparison tests.

3. Results and discussion

3.1. Surface characterization

TEM and HRTEM images of GNR, Au@Ag, Au@Pt, and Au@Ag@Pt are shown in Figure 1. GNR presents a smooth nanorod morphology with the length of 55.9±6.1 nm, the width of 16.6±2.3 nm, and length/width (L/D) ratio of approximately 3.4. Lattice fringes can be clearly observed which suggests that GNR has good crystallinity. TEM morphology with apparent core-shell nanorod structure can be seen from Au@Ag with the length of 58.6±7.4 nm, the width of 20.0±3.5 nm, and an *L/D* ratio of approximately 2.9. Components of Au and Ag elements were detected from Au@Ag by EDS analysis as shown in Table 1. Based on these, it can be concluded that the Ag shell layer has been successfully fabricated on gold nanorod surface. Besides, with the lattice parameters of Au and Ag being similar, there is a smooth and flat interface between the Au core and the Ag shell. Au and Pt elements were detected from Au@Pt (Table 1) which suggests that Pt can be deposited on gold nanorod surface with chemical reduction method. However, the Pt was unevenly distributed on gold nanorod with island structures as presented in Figure 1, which is ascribed to the high surface energy and cohesive energy of Pt [19]. Table 1 shows that Au, Ag, and Pt were detected from Au@Ag@Pt which implies that Pt has been successfully deposited on Au@Ag@Pt. Similarly, Pt on Au@Ag@Pt exhibits island structure.

UV-Vis-NIR absorption spectra of GNR, Au@Ag, Au@Pt, and Au@Ag@Pt are shown in Figure 2. Two apparent absorption peaks at 520 nm and 808 nm are observed from GNR which correspond to the transverse plasma resonance absorption peak (TPRAP) and longitudinal plasma resonance absorption peak (LPRAP), respectively. TPRAP is relatively steady, while LPRAP is susceptible to the changes of

physicochemical properties of gold nanorod including surface roughnesses, *L/D* ratios, and so on [19]. Compared with GNR, the TPRAP of Au@Ag has no significant change while the LPRAP shows a blue shift which is ascribed to the reduction of the *L/D* ratio. The LPRAP is closely related to the *L/D* ratio of gold nanorod that it will show a blue shift with the decrease of *L/D* ratio [20]. However, LPRAP of Au@Pt and Au@Ag@Pt exhibit red shift due to the large surface roughness [21].

GNR, Au@Ag, Au@Pt, and Au@Ag@Pt were assembled on the titanium surface and corresponding SEM surface morphologies of Ti, Ti-GNR, Ti-Au@Ag, Ti-Au@Pt, and Ti-Au@Ag@Pt are presented in Figure 3. Ti shows a relatively flat surface at low magnification and honeycomb nanostructures can be observed at high magnification due to the etching effect of piranha solution. GNR, Au@Ag, Au@Pt, and Au@Ag@Pt are uniformly distributed on the titanium surface where rod-like structures can be seen. XPS full spectra and composition percentage analysis of Ti, Ti-GNR, Ti-Au@Ag, Ti-Au@Pt, and Ti-Au@Ag@Pt are shown in Figure 4a and Table 2, respectively. C elements are detected from all the samples due to carbon contamination. Ti and O elements are detected from the Ti sample which may be ascribed to the formation of titanium oxide during the cleaning process using piranha solution. Ag elements are observed from Ti-Au@Ag and Ti-Au@Ag@Pt, Pt elements can be seen from Ti-Au@Pt and Ti-Au@Ag@Pt, and Au elements appear on Ti-GNR, Ti-Au@Ag, Ti-Au@Pt, and Ti-Au@Ag@Pt. It further confirms that GNR, Au@Ag, Au@Pt, and Au@Ag@Pt have been successfully fabricated on the titanium surface. Besides, chemical states of Au, Ag, and Pt on Ti-Au@Ag@Pt were investigated and

corresponding results of XPS high-resolution spectra are presented in Figure 4(b-d). Binding energy at 83.6 eV and 87.3 eV correspond to the Au 4f 7/2 and Au 4f 5/2 in metallic gold, respectively [22]. The high-resolution spectra of Ag 3d and Pt 4f also verify the presence of metallic silver and platinum [23, 24].

3.2. Surface wettability

Nanorods of GNR, Au@Ag, Au@Pt and Au@Ag@Pt on titanium surface have an effect on the surface wettability as shown in Figure 5. Ti exhibits a hydrophilic surface with a contact angle of 3.3° due to the existence of hydroxyl resulting from pickling using piranha solution. Compared with Ti, contact angles of Ti-GNR, Ti-Au@Ag, Ti-Au@Pt and Ti-Au@Ag@Pt increase and there are no significant differences among them.

3.3. Ag release analysis

Ag release features from Ti-GNR, Ti-Au@Ag, Ti-Au@Pt, and Ti-Au@Ag@Pt within 7 days were investigated and the results are presented in Table 3. Ag element was not detected from Ti-GNR and Ti-Au@Pt. Ag contents released from Ti-Au@Ag and Ti-Au@Ag@Pt with 7 days are 0.0156 μg/mL and 0.0055 μg/mL, respectively. Compared with Ti-Au@Ag, there was less Ag content released from Ti-Au@Ag@Pt. It indicates that the Pt shell layer on Ti-Au@Ag@Pt can regulate the Ag ions release in a slow way.

3.4. Antibacterial activity assessment

Strains of *S. epidermidis* and *P. aeruginosa* were used to assess the antibacterial activities of Ti, Ti-GNR, Ti-Au@Ag, Ti-Au@Pt, and Ti-Au@Ag@Pt and surface

morphologies of bacteria cultured on various samples are shown in Figure 6a. *S. epidermidis* shows a smooth and intact spherical morphology on Ti which indicates that Ti has no antibacterial activity against *S. epidermidis*. A few *S. epidermidis* with deformed morphology can be observed from Ti-GNR and Ti-Au@Pt, and most *S. epidermidis* grow well on Ti-GNR and Ti-Au@Pt. However, the bacteria numbers of *S. epidermidis* on Ti-Au@Ag and Ti-Au@Ag@Pt were significantly reduced and most *S. epidermidis* were dead with wizened morphology (red arrows), especially for Ti-Au@Ag. It suggests that Ti-Au@Ag and Ti-Au@Ag@Pt have good antibacterial activity against *S. epidermidis*. A similar antibacterial effect can be found on *P. aeruginosa* cultured on Ti, Ti-GNR, Ti-Au@Ag, Ti-Au@Pt, and Ti-Au@Ag@Pt for 24 h. *P. aeruginosa* grew well on Ti and a few *P. aeruginosa* with deformed morphology could be found on Ti-GNR and Ti-Au@Pt. However, *P. aeruginosa* on Ti-Au@Ag and Ti-Au@Ag@Pt were dead with malformed cell morphology, especially for Ti-Au@Ag. To further calculate the antibacterial rates of Ti, Ti-GNR, Ti-Au@Ag, Ti-Au@Pt, and Ti-Au@Ag@Pt against *S. epidermidis* and *P. aeruginosa*, plate colony counting was performed and the results are shown in Figure 6(b and c). The antibacterial rates of Ti-GNR, Ti-Au@Ag, Ti-Au@Pt, and Ti-Au@Ag@Pt against *S. epidermidis* are 48.0%, 57.0%, 98.0%, and 89.7, respectively. The antibacterial rates of Ti-GNR, Ti-Au@Ag, Ti-Au@Pt, and Ti-Au@Ag@Pt against *P. aeruginosa* are 19.3%, 32.9%, 100%, and 92.7, respectively. It indicates that Ti-Au@Ag exhibits the highest antibacterial activity, followed by Ti-Au@Ag@Pt. To further investigate the Ag release antibacterial effect, agar diffusion assay was performed and the results are presented in Figure 7. Inhibition

zones can only be found on Ti-Au@Ag and Ti-Au@Ag@Pt. The inhibition zone diameters of Ti-Au@Ag and Ti-Au@Ag@Pt against *S. epidermidis* were measured at 2.35 cm and 1.81 cm, respectively, and the inhibition zone diameters of Ti-Au@Ag and Ti-Au@Ag@Pt against *P. aeruginosa* were measured at 3.23 cm and 1.91 cm, respectively. It implies that Au@Ag and Ti-Au@Ag@Pt can kill bacteria by releasing Ag ions.

Antibacterial mechanisms of Ag-based antibacterial agents have been widely investigated. Cao et al. introduced Ag nanoparticles into titanium substrate using plasma immersion ion implantation technique and demonstrated the controlled antibacterial activity resulting from micro-galvanic effects between Ag nanoparticles and titanium matrix [23]. Nevertheless, many studies reported that released Ag ions from Ag-based antibacterial agents played a vital role in antibacterial activity [25-28]. Ag^0 nanoparticles would not exist long in a realistic environment where H^+ and dissolved O_2 could oxidize Ag^0 nanoparticles to release Ag ions [29]. In this present study, released Ag ions were detected from Ti-Au@Ag and Ti-Au@Ag@Pt and inhibition zones could also be found around Ti-Au@Ag, and Ti-Au@Ag@Pt by agar diffusion assay, which confirmed the antibacterial mechanism of Ag ions release. Besides, the Pt shell layer on Ti-Au@Ag@Pt could regulate the Ag ions release in a slow way.

3.5. Biocompatibility evaluation

MC3T3-E1 cells were utilized to assess the biocompatibility of Ti, Ti-GNR, Ti-Au@Ag, Ti-Au@Pt, and Ti-Au@Ag@Pt and SEM surface morphologies of MC3T3-

E1 cells cultured on various samples for 1 day are presented in Figure 8. A lot of cells adhered on the sample surfaces can be found from Ti, Ti-GNR, and Ti-Au@Pt at low magnification, and filopodia and lamellipodia can be seen at high magnification. However, the number of cells grown on Ti-Au@Ag was little and cells were almost dead with spherical morphology. Compared with Ti-Au@Ag, the number of cells on Ti-Au@Ag@Pt increased, and filopodia and lamellipodia were observed. As presented in Table 3, compared with Ti-Au@Ag, the Pt shell layer on Ti-Au@Ag@Pt slows down the Ag ions release rate. Therefore, Ti-Au@Ag@Pt shows no obvious cell toxicity where MC3T3-E1 cells grow well on the sample surface.

4. Conclusion

In summary, Au@Ag@Pt core-shell nanorods were fabricated on the titanium surface. Compared with Ti-Au@Ag, Ti-Au@Ag@Pt remained the antibacterial activities against *S. epidermidis* and *P. aeruginosa*. Moreover, Ti-Au@Ag@Pt shows no obvious cell toxicity where MC3T3-E1 cells grow well on the sample surface. Pt shell layer on Ti-Au@Ag@Pt slows down the Ag ion release rate which endows medical titanium surface both antibacterial activity and good biocompatibility.

Acknowledgements

Financial support from the National Natural Science Foundation of China (No. 51831011), Shanghai Scientific and Technological Innovation Project (20ZR1452200), Program for Outstanding Medical Academic Leader (2019LJ27), the PhD Research Startup Foundation of Jiamusi University (No. JMSUBZ2019-09), Shanghai Medical

Key Specialty (ZK2019B12), China Postdoctoral Science Foundation (No. 2019M661642).

Declaration of interests

The authors declare no competing financial interests.

References

[1] X.Y. Liu, P.K. Chu, C.X. Ding, Surface modification of titanium, titanium alloys, and related materials for biomedical applications, Mat Sci Eng R 47(3-4) (2004) 49-121.

[2] J.Q. Liu, J. Liu, S. Attarilar, C. Wang, M. Tamaddon, C.L. Yang, K.G. Xie, J.G. Yao, L.Q. Wang, C.Z. Liu, Y.J. Tang, Nano-Modified Titanium Implant Materials: A Way Toward Improved Antibacterial Properties, Front Bioeng Biotech 8 (2020).

[3] V. Ständert, K. Borcherding, N. Bormann, G. Schmidmaier, I. Grunwald, B. Wildemann, Antibiotic-loaded amphora-shaped pores on a titanium implant surface enhance osteointegration and prevent infections, Bioactive materials 6(8) (2021) 2331-2345.

[4] W.H. Qian, J.J. Qiu, J.S. Su, X.Y. Liu, Minocycline hydrochloride loaded on titanium by graphene oxide: an excellent antibacterial platform with the synergistic effect of contact-killing and release-killing, Biomater Sci-Uk 6(2) (2018) 304-313.

[5] J. Qiu, L. Liu, H. Zhu, X. Liu, Combination types between graphene oxide and substrate affect the antibacterial activity, Bioactive materials 3(3) (2018) 341-346.

[6] X. Yan, S. Li, J. Bao, N. Zhang, B. Fan, R. Li, X. Liu, Y.-X. Pan, Immobilization of Highly Dispersed Ag Nanoparticles on Carbon Nanotubes Using Electron-Assisted Reduction for Antibacterial Performance, ACS applied materials & interfaces 8(27) (2016) 17060-17067.

[7] Z. Xu, M. Li, X. Li, X. Liu, F. Ma, S. Wu, K.W.K. Yeung, Y. Han, P.K. Chu, Antibacterial Activity of Silver Doped Titanate Nanowires on Ti Implants, ACS applied materials & interfaces 8(26) (2016) 16584-16594.

[8] J. Qiu, D. Wang, H. Geng, J. Guo, S. Qian, X. Liu, How Oxygen-Containing Groups on Graphene Influence the Antibacterial Behaviors, Adv Mater Interfaces 4(15) (2017) 1700228.

[9] M. Frieri, K. Kumar, A. Boutin, Antibiotic resistance, Journal of Infection and Public Health 10(4) (2017) 369-378.

[10] J. Shang, Y. Sun, T. Zhang, Z. Liu, H. Zhang, Enhanced Antibacterial Activity of Ag Nanoparticle-Decorated ZnO Nanorod Arrays, J Nanomater 2019 (2019).

[11] Q. Liu, J. Li, X. Zhong, Z. Dai, Z. Lu, H. Yang, R. Chen, Enhanced antibacterial activity and mechanism studies of Ag/Bi2O3 nanocomposites, Advanced Powder Technology 29(9) (2018) 2082-2090.

[12] C.-C. Chen, H.-H. Wu, H.-Y. Huang, C.-W. Liu, Y.-N. Chen, Synthesis of High Valence Silver-Loaded Mesoporous Silica with Strong Antibacterial Properties, Int J Env Res Pub He 13(1) (2016).

[13] B. Chen, Y. Jiang, M. Zhao, W. Wang, Z. Chu, R. Huo, F. Hu, W. Zhou, T. He, H. Qian, Ag nanoparticles decorated hybrid microspheres for superior antibacterial properties, Materials Letters 262 (2020).

[14] W. Fan, D. Wu, T. Ma, B. Fan, Ag-loaded mesoporous bioactive glasses against Enterococcus faecalis biofilm in root canal of human teeth, Dental Materials Journal 34(1) (2015) 54-60.

[15] L. Wei, H. Wang, Z. Wang, M. Yu, S. Chen, Preparation and long-term antibacterial activity of TiO2 nanotubes loaded with Ag nanoparticles and Ag ions, Rsc Adv 5(91) (2015) 74347-74352.

[16] X.Y. Yang, A.P. Gondikas, S.M. Marinakos, M. Auffan, J. Liu, H. Hsu-Kim, J.N. Meyer, Mechanism of Silver Nanoparticle Toxicity Is Dependent on Dissolved Silver and Surface Coating in Caenorhabditis elegans, Environ Sci Technol 46(2) (2012) 1119-1127.

[17] Z.M. Xiu, Q.B. Zhang, H.L. Puppala, V.L. Colvin, P.J.J. Alvarez, Negligible Particle-Specific Antibacterial Activity of Silver Nanoparticles, Nano letters 12(8) (2012) 4271-4275.

[18] T. Yang, D. Wang, X. Liu, Assembled gold nanorods for the photothermal killing of bacteria, Colloid Surface B 173 (2019) 833-841.

[19] E. Bus, J.A. van Bokhoven, Electronic and geometric structures of supported platinum, gold, and platinum - Gold catalysts, J Phys Chem C 111(27) (2007) 9761-9768.

[20] H.J. Chen, L. Shao, Q. Li, J.F. Wang, Gold nanorods and their plasmonic properties, Chemical Society reviews 42(7) (2013) 2679-2724.

[21] X.N. Hu, Y.Y. Zhao, Z.J. Hu, A. Saran, S. Hou, T. Wen, W.Q. Liu, Y.L. Ji, X.Y. Jiang, X.C. Wu, Gold nanorods core/AgPt alloy nanodots shell: A novel potent antibacterial nanostructure, Nano research 6(11) (2013) 822-835.

[22] J.G. Yu, L. Yue, S.W. Liu, B.B. Huang, X.Y. Zhang, Hydrothermal preparation and photocatalytic activity of mesoporous Au-TiO2 nanocomposite microspheres, Journal of colloid and interface science 334(1) (2009) 58-64.

[23] H.L. Cao, X.Y. Liu, F.H. Meng, P.K. Chu, Biological actions of silver nanoparticles embedded in titanium controlled by micro-galvanic effects, Biomaterials 32(3) (2011) 693-705.

[24] O. Kerrec, D. Devilliers, H. Groult, P. Marcus, Study of dry and electrogenerated Ta2O5 and Ta/Ta2O5/Pt structures by XPS, Mat Sci Eng B-Solid 55(1-2) (1998) 134-142.

[25] P. Saint-Cricq, J.Z. Wang, A. Sugawara-Narutaki, A. Shimojima, T. Okubo, A new synthesis of well-dispersed, core-shell Ag@SiO2 mesoporous nanoparticles using amino acids and sugars, Journal of Materials Chemistry B 1(19) (2013) 2451-2454.

[26] C. Li, X.S. Wang, F. Chen, C.L. Zhang, X. Zhi, K. Wang, D.X. Cui, The antifungal activity of graphene oxide-silver nanocomposites, Biomaterials 34(15) (2013) 3882-3890.

[27] N. Gao, Y.J. Chen, J. Jiang, Ag@Fe2O3-GO Nanocomposites Prepared by a Phase Transfer Method with Long-Term Antibacterial Property, ACS applied materials & interfaces 5(21) (2013) 11307-11314.

[28] X. Yan, S. Li, Y. Pan, B. Xing, R. Li, B.W.L. Jang, X. Liu, Tunable Ag+ ion release from Ag@C for antibacterial and antifouling performances, Rsc Adv 5(49) (2015) 39384-39391.

[29] J.Y. Liu, R.H. Hurt, Ion Release Kinetics and Particle Persistence in Aqueous Nano-Silver Colloids, Environ Sci Technol 44(6) (2010) 2169-2175.

Figure and table captions

Fig. 1. TEM and HRTEM images of GNR, Au@Ag, Au@Pt and Au@Ag@Pt. The scale bar is 20 nm.

Fig. 2. UV-Vis-NIR spectra of GNR, Au@Ag, Au@Pt and Au@Ag@Pt.

Fig. 3. SEM images of Ti, Ti-GNR, Ti-Au@Ag, Ti-Au@Pt and Ti-Au@Ag@Pt at low and high magnification. The scale bars are 1 μm and 300 nm which correspond to the low and high magnification, respectively.

Fig. 4. XPS full spectra of Ti, Ti-GNR, Ti-Au@Ag, Ti-Au@Pt and Ti-Au@Ag@Pt (a); Au (b), Ag (c) and Pt (d) high-resolution spectra of Ti-Au@Ag@Pt.

Fig. 5. Water contact angles of Ti, Ti-GNR, Ti-Au@Ag, Ti-Au@Pt and Ti-Au@Ag@Pt. $^{***}P < 0.001$ vs. Ti.

Fig. 6. SEM morphologies of *S. epidermidis* and *P. aeruginosa* on Ti, Ti-GNR, Ti-Au@Ag, Ti-Au@Pt and Ti-Au@Ag@Pt. The red arrows indicate the damaged bacteria (a); antibacterial rate of Ti, Ti-GNR, Ti-Au@Ag, Ti-Au@Pt and Ti-Au@Ag@Pt against *S. epidermidis* (b) and *P. aeruginosa* (c) based on the plate colony counting method. The scale bar is 5 μm, $^{**}p < 0.01$, $^{***}p < 0.001$.

Fig. 7. Inhibition zones around Ti, Ti-GNR, Ti-Au@Ag, Ti-Au@Pt and Ti-Au@Ag@Pt against *S. epidermidis* and *P. aeruginosa*. The red circle indicates the inhibition zone.

Fig. 8. SEM morphologies of MC3T3-E1 cells cultured on Ti, Ti-GNR, Ti-Au@Ag, Ti-Au@Pt and Ti-Au@Ag@Pt for 1 day. The scale bar is 200 μm.

Tab. 1. EDS component analysis and the ratio of Ag/Au and Pt/Au of Au@Ag、Au@Pt、Au@Ag@Pt.

Tab. 2. XPS component analysis of Ti-GNR, Ti-Au@Ag, Ti-Au@Pt, and Ti-Au@Ag@Pt.

Tab. 3. Release contents of Ag from Ti-GNR, Ti-Au@Ag, Ti-Au@Pt and Ti-Au@Ag@Pt within 7 days.

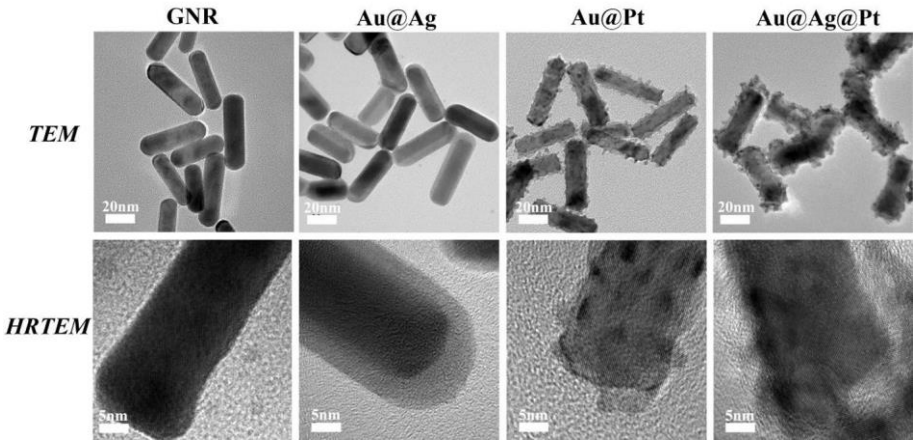

Figure 1

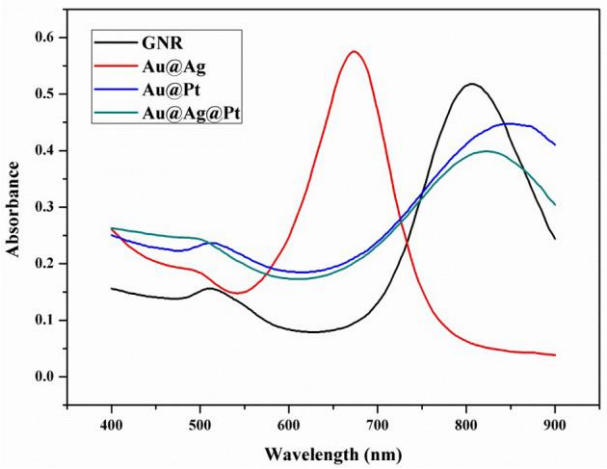
GNR
Au@Ag
Au@Pt
Au@Ag@Pt
Absorbance
Wavelength (nm)
0.0
0.1
0.2
0.3
0.4
0.5
0.6
400
500
600
700
800
900

Figure 2

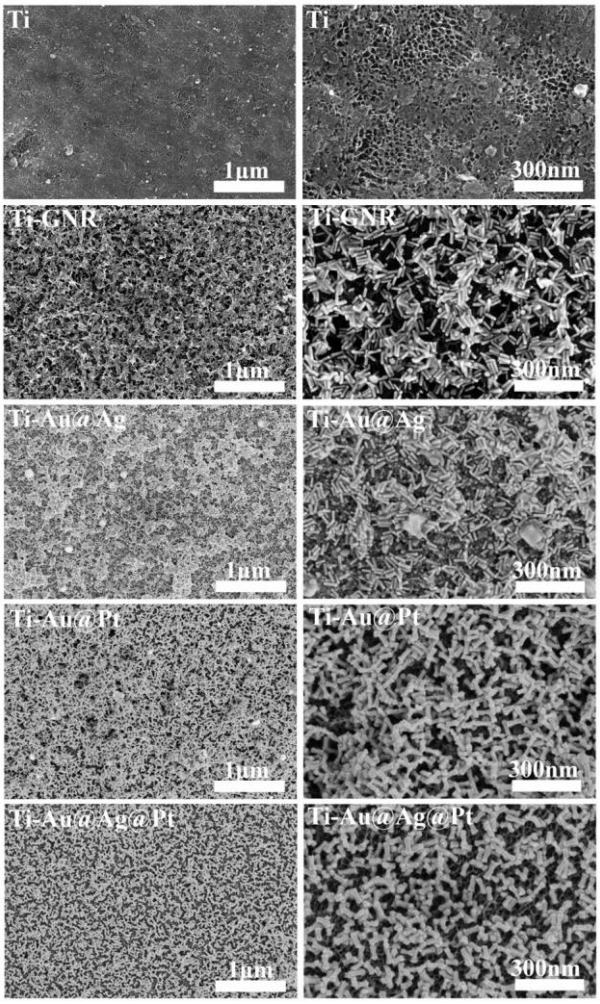
Ti
1μm
Ti
300nm
Ti-GNR
1μm
Ti-GNR
300nm
Ti-Au@Ag
1μm
Ti-Au@Ag
300nm
Ti-Au@Pt
1μm
Ti-Au@Pt
300nm
Ti-Au@Ag@Pt
1μm
Ti-Au@Ag@Pt
300nm

Figure 3

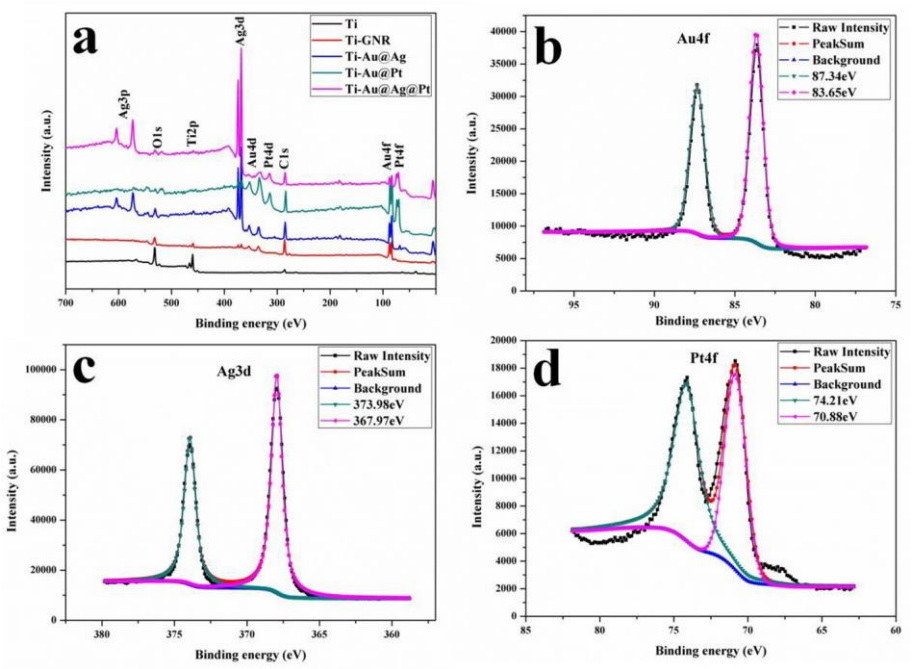
a
Ti
Ti-GNR
Ti-Au@Ag
Ti-Au@Pt
Ti-Au@Ag@Pt
Ag3p
O1s
Ti2p
Ag3d
Au4d
Pt4d
C1s
Au4f
Pt4f
Intensity (a.u.)
Binding energy (eV)
b
Au4f
Raw Intensity
PeakSum
Background
87.34eV
83.65eV
Intensity (a.u.)
Binding energy (eV)
c
Ag3d
Raw Intensity
PeakSum
Background
373.98eV
367.97eV
Intensity (a.u.)
Binding energy (eV)
d
Pt4f
Raw Intensity
PeakSum
Background
74.21eV
70.88eV
Intensity (a.u.)
Binding energy (eV)

Figure 4

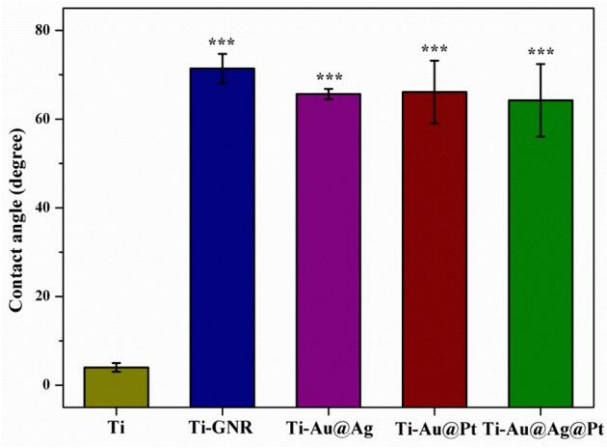
Contact angle (degree)
80
60
40
20
0
***
***
***
***
Ti
Ti-GNR
Ti-Au@Ag
Ti-Au@Pt
Ti-Au@Ag@Pt

Figure 5

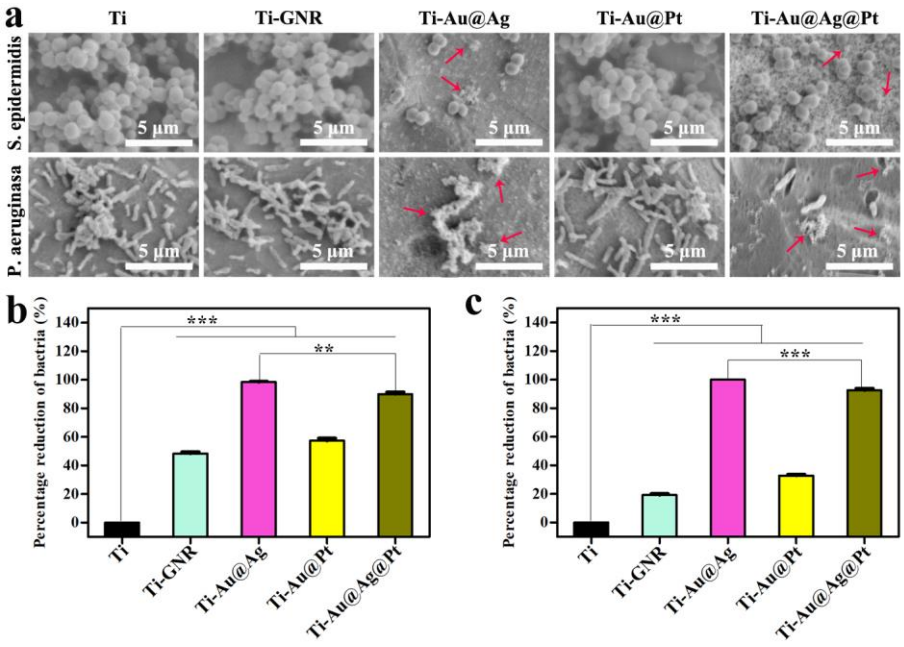
a
Ti
Ti-GNR
Ti-Au@Ag
Ti-Au@Pt
Ti-Au@Ag@Pt
S. epidermidis
P. aeruginasa
5 μm
b
c
Percentage reduction of bactria (%)
***
**
***
Ti
Ti-GNR
Ti-Au@Ag
Ti-Au@Pt
Ti-Au@Ag@Pt

Figure 6

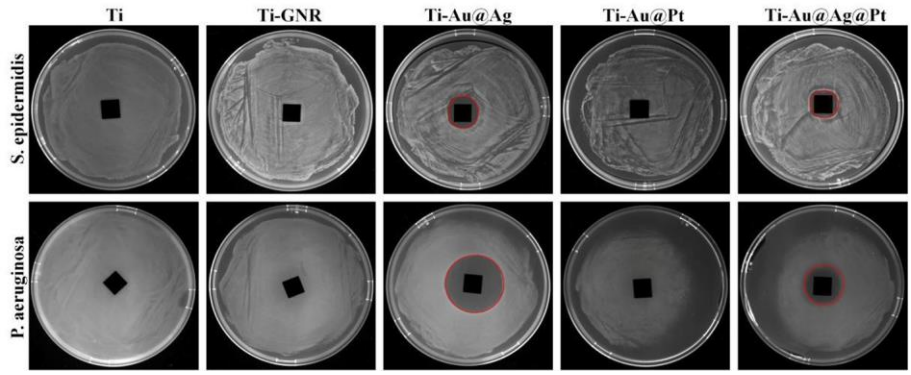
Ti
Ti-GNR
Ti-Au@Ag
Ti-Au@Pt
Ti-Au@Ag@Pt
S. epidermidis
P. aeruginosa

Figure 7

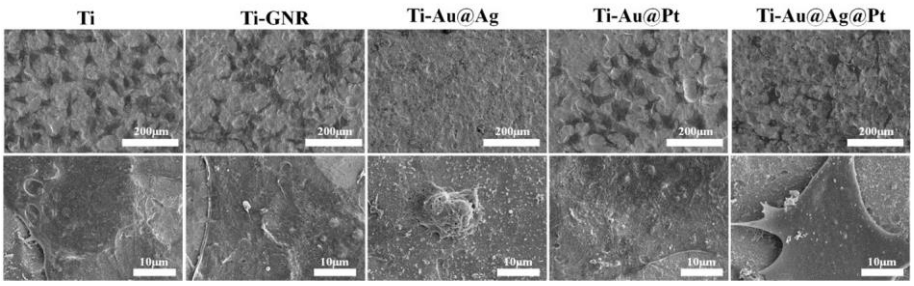

Figure 8

Table 1

Samples	Atomic ratio (%)		
	Au	Ag	Pt
Au@Ag	53.52	46.48	-
Au@Pt	75.84	-	24.16
Au@Ag@Pt	48.56	30.13	21.31

Table 2

Samples	Atomic ratio (%)					
	C	O	Ti	Au	Ag	Pt
Ti-GNR	64.61	21.70	4.42	9.27	-	-
Ti-Au@Ag	60.60	23.41	4.37	6.22	5.40	-
Ti-Au@Pt	62.31	13.04	1.98	17.19	-	5.48
Ti-Au@Ag@Pt	70.79	8.60	1.03	9.51	5.90	4.17

Table 3

Samples	Ti-GNR	Ti-Au@Ag	Ti-Au@Pt	Ti-Au@Ag@Pt
Content (μg/mL)	-	0.0156 ± 0.0037	-	0.0055 ± 0.0019